Papers in Physics, vol. 16, art. 160001 (2024)

www.papersinphysics.org

Received: 09 May 2024, Accepted: 09 August 2024
Edited by: L. Foini
Reviewed by: A.B. Kolton, Bariloche Atomic Centre, Argentina
Licence: Creative Commons Attribution 4.0
DOI: https://doi.org/10.4279/PIP.160001

ISSN 1852-4249

On the spontaneous magnetization of two-dimensional ferromagnets

D. Pescia,[1*] A. Vindigni[1,2†]

Ferromagnetism is typically discussed in terms of the exchange interaction and magnetic anisotropies. Yet real samples are inevitably affected by the magnetostatic dipole-dipole interaction. Because of this interaction, a theorem [R.B. Griffiths, Free Energy of interacting magnetic dipoles, *Phys. Rev.* 176, 655 (1968)] forbids a spontaneous magnetization in, nota bene, three-dimensional bodies. Here we discuss perpendicularly and in-plane magnetized ferromagnetic bodies in the shape of a slab of finite thickness. In perpendicularly magnetized slabs, magnetic domains are energetically favored when the lateral size is sufficiently large, i.e., there is no spontaneous magnetization. For in-plane magnetization, instead, spontaneous magnetization is possible below a critical thickness which, in very thin films, could be as small as few monolayers. At this critical thickness, we predict a genuine phase transition to a multi-domain state. These results have implications for two-dimensional ferromagnetism.

I Introduction

A familiar situation in ferromagnetism foresees that, below the Curie temperature, the graph of the free-energy as a function of the magnetization has a flat portion [1] (graph "a" in Fig. 1). This flatness defines a situation in which the magnetization can acquire a value between zero and a so-called "spontaneous magnetization" $\pm M_s$ without any change in the free energy. This "flatness" is a property of the thermodynamic limit, i.e., of infinite bodies. In finite bodies, the free energy assumes a shape that resembles the graph "b" in Fig. 1, $\pm M_s$ being the values at which the free energy has minima. Systems with spontaneous magnetization are, for example, the Ising and classical Heisenberg ferromagnets in three dimensions (3D) [1,2], the 2D-Ising model or the 2D-planar and classical 2D-Heisenberg models with symmetry breaking single-ion interactions [3]. In real ferromagnetic bodies, however, the inevitable dipole-dipole interaction, originating within Maxwell's equations for magnetostatics, must be considered alongside the main exchange interaction (of purely quantum mechanical origin) and the single-ion magnetic anisotropies (produced by the spin-orbit interaction). The dipole-dipole interaction is, typically, much weaker than the exchange interaction (by about two orders of magnitude). Yet, it is long-ranged, as it decays only with the third power of the distance between two magnetic moments. Because of the dipole-dipole interaction, a theorem, proved by Griffiths [4] for bodies with linear dimension L approaching infinity along all three spatial dimensions, implies that any non-zero magnetization produces an increase of the free energy, i.e., the graph of the free energy as a function of M has a minimum at $M = 0$ at any temperature (graph "c" in Fig. 1). Accordingly, ferromagnetic order

* pescia@phys.ethz.ch
† vindigni@phys.ethz.ch

[1] Laboratory for Solid State Physics, ETH Zurich, 8093 Zurich, Switzerland

[2] Department of Evolutionary Biology and Environmental Studies, University of Zurich, 8057 Zurich, Switzerland.

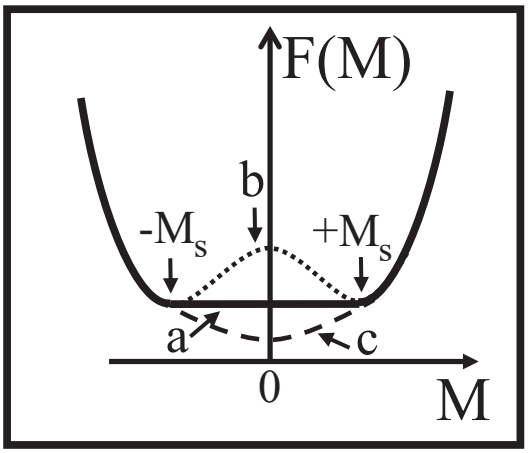

Figure 1: The free energy F as a function of M. a: The graph for an infinite ferromagnetic body with spontaneous magnetization has a flat portion between $\pm M_s$ below the Curie temperature (see Ref.[1]). b: For a finite ferromagnetic body, the free energy has minima at $\pm M_s$. c: A theorem by Griffiths [4] implies that the free energy has a minimum at $M = 0$ at any temperature.

can only be local and, globally, the spontaneous magnetization is exactly vanishing.

This no-spontaneous magnetization rule is somewhat similar to the absence of long-range order foreseen for the isotropic 2D-planar and 2D-Heisenberg ferromagnets [5] but it refers, remarkably, to a 3D-body. In fact, it appears that an important assumption underlying Griffith's theorem is the size of the body approaching infinity along all three spatial dimensions. In this paper, we discuss ferromagnetism in the presence of exchange, magnetic anisotropy and dipole-dipole interaction, but in a thin film geometry, where only two spatial dimensions are allowed to increase and the third is assigned a finite thickness. Our results should be relevant for discussing ferromagnetism in the new class of monolayer thin materials obtained by mechanical exfoliation [6–11]. They are known to be perfectly flat over large distances and have been shown to be vertically engineerable [12]. As experiments are often analyzed in term of abstract models, exact theorems such as Griffiths's [4] or scaling arguments such as those presented here should allow experiments to distinguish those features that are general and universal from those that originate from less known details of a sample (such as defects).

Before we proceed, we describe the general assumptions underlying all our arguments. We model a thin film by a slab with area L^2 and thickness $d \ll L$. The slabs host a continuous magnetization distribution. The use of a continuous model requires establishing a link to "real" samples, which host magnetic moments on a lattice. We establish the link by assuming that the magnetization is measured in units of $M_0 \doteq \frac{g \cdot \mu_B \cdot S}{a^3}$, thereby introducing the atomic scale quantities g (the g-factor), S (the spin at a lattice site, in units of $\hbar$) and a (the lattice constant for a simple cubic lattice). By these assumptions, the thickness of the slab corresponding to "1 Monolayer" (1ML) is a. Finally, we assume that the magnetization is independent of the coordinate z perpendicular to the film plane. We will comment on this assumption in Section IV.

II Perpendicular magnetization

We first analyze the situation of perpendicular magnetization. In the state of spontaneous perpendicular magnetization, all magnetic moments in the slab point along one of the two z-directions perpendicular to the slab (Fig. 2a), e.g., the $+z$-direction. In Fig. 2a, this state is rendered with a white color and the magnetization vector with absolute value M_0 is given by a black arrow. A possible, elementary state of vanishing spontaneous magnetization is shown in Fig. 2b. One half of the slab is still filled with magnetic moments pointing upwards ("↑") but the other half (gray in Fig. 2b) contains magnetic moments pointing downwards ("↓") (indicated as state ↑↓ henceforth). Assuming that Griffith's theorem is valid for the perpendicular magnetization in the slab geometry as well, the ↑↓ state should have a lower total energy than the state of spontaneous uniform magnetization (indicated as state ↑↑ henceforth).

i The magnetostatic energy

The magnetostatic energy E_M for the perpendicular magnetization configuration is most appropriately computed as the energy of the interacting Ampèrian effective current densities $\vec{\nabla} \times \vec{M}(\vec{r})$ resulting from the magnetization vector $\vec{M}(\vec{r})$ (see Section I of the Supplementary Material (SM)). The current density vectors arising in the ↑↑ and ↑↓ configurations are summarized by red arrows in

Fig. 2. We find that the formation of the two neighboring domains with opposite magnetization lowers the total magnetostatic energy and is thus the driving force behind the suppression of the spontaneous magnetization, i.e., $E_M(\uparrow\downarrow) - E_M(\uparrow\uparrow)$ is negative. The self-energies of the Ampèrian currents circulating along the perimeter of the slab cancel out exactly from $E_M(\uparrow\downarrow) - E_M(\uparrow\uparrow)$. Their mutual interaction provides terms of the order $L \cdot d^2$. The leading contribution to $E_M(\uparrow\downarrow) - E_M(\uparrow\uparrow)$ is the self-energy of the current flowing along the wall that separates the domains. Assuming that the domain wall has a thickness w, the leading contribution of $E_M(\uparrow\downarrow) - E_M(\uparrow\uparrow)$ is proportional to (Section I, SM),

$$-\frac{L \cdot d}{a^2} \cdot \frac{2}{\pi} \cdot \left(\Omega \cdot \frac{d}{a}\right) \cdot \ln\left(\frac{L}{w}\right), \qquad (1)$$

in the limit $d \ll w \ll L$. In Eq. 1, $L \cdot d$ is the surface of the domain wall. $\Omega \doteq \frac{\mu_0}{2} \cdot M_0^2 \cdot a^3$ is a parameter used for expressing the strength of the magnetostatic energy per unit volume cell (we refer to Section I of SM and the Tables in Section IV for representative values of Ω and the further parameters introduced in this paper). The slab model (see Section I of SM) shows explicitly that the relevant coupling constant entering $E_M(\uparrow\downarrow) - E_M(\uparrow\uparrow)$ is not Ω itself, but $\Omega \cdot \frac{d}{a}$, i.e., the characteristic magnetostatic energy per unit surface cell. The logarithmic term in Eq. 1 provides, formally, a divergence of $E_M(\uparrow\downarrow) - E_M(\uparrow\uparrow)$ with the size L. It is universal in the sense that it does not depend on the exact geometry of the wall separating the domains: both the shape of this wall and the exact shape of the slab contribute only terms of the order $\Omega \cdot L \cdot d^2$.

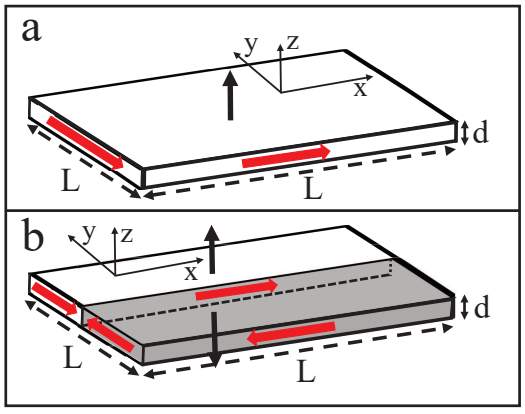

Figure 2: a: The state of uniform perpendicular magnetization (represented in white) in a slab. The magnetization vector is represented by the vertical black arrow. Red arrows represent the effective current density vectors flowing along the perimeter of the slab. b: The slab is filled by two domains with magnetization vector parallel (white domain) and antiparallel (gray domain) to the vertical z-axis. Red arrows represent the effective current density vectors.

A technical aspect: the integrals of Section I of SM can be managed to cover the case $d \gg w$. In this limit, d replaces w in the argument of the logarithm of Eq. 1. The case of $d \approx w$ is more subtle. Given the fact that the cross section of the wire carrying the effective current is $d \cdot w$, we heuristically assume that $\approx \sqrt{d \cdot w}$ appears in the argument of the logarithm. Later, (see Eq. 2), we will show that w depends on various material parameters and diverges in some situations, so that we will continue our discussion having the "ultrathin" limit $d \ll w$ in mind, as d is one parameter that is defined by the experiment, not by the material.

ii The energy of the domain wall

The formation of a domain wall in the $\uparrow\downarrow$-state increases the total energy of the ferromagnetic slab and therefore promotes the state of spontaneous magnetization. For simplicity, we assume the wall to run parallel to the x-direction and the rotation to take place along the y-direction. We now list the various energies involved in the formation of the wall.

Néel single-ion magnetic anisotropy. Within the wall, the magnetic moments rotate away from the z-direction. Let the rotation be characterized by an angle θ, which increases from 0 to π when moving along y within the wall. The misalignment is associated, in the first place, with an increase of the single-ion magnetic anisotropy energy that favors the perpendicular magnetization introduced conceptually by Néel [13] and computed for the first time from first principles by Gay and Richter [14] for the monolayer of Fe. This anisotropy originates from the breaking of translational symmetry perpendicular to the film. It is, accordingly, proportional to $\cos^2\theta(y)$. We call the proportionality constant $-\lambda$, the negative sign indicating that this anisotropy favors the state of perpendicular magnetization. As this anisotropy is located mainly at

the two surfaces bounding the thin film, the proportionality constant λ scales with the area of the film, not with its volume [15]. Accordingly, λ is only weakly dependent on d [15]. Actually, spin wave excitations produce a temperature and d dependence of λ and Ω [16, 17]. This will have an impact on the crossover length to a multidomain state (see later in the paper).

The magnetostatic energy. The magnetostatic energy itself favors the magnetic moment to lie within the slab plane and contributes a term $+\Omega\cdot\frac{d}{a}\cdot\cos^2\theta(y)$ (Section II of SM). In contrast to λ, the coefficient of the dipolar contribution scales with d (see Section II of SM and Ref. [15]).

The exchange energy. Finally, for the building of the wall, one must also consider that the misalignment of two neighboring magnetic moments at the sites y and $y\pm a$ increases the energy by [18] $J\cdot S^2\cdot\cos\left(\theta(y\pm a)-\theta(y)\right)$, J being the exchange coupling energy per spin couple. In Section III of the SM, we find an expression for the equilibrium width w of the domain wall and for its total energy E_w which includes λ, J and the magnetostatic contribution:

$$w_\perp = \frac{a}{2}\sqrt{\frac{2\cdot J\cdot S^2}{\lambda-\Omega\frac{d}{a}}}, \tag{2}$$

$$E_{w_\perp} = \frac{L\cdot d}{a^2}\cdot\left[2\cdot\sqrt{\left(\lambda-\Omega\cdot\frac{d}{a}\right)\cdot 2\cdot J\cdot S^2}\right], \tag{3}$$

(when necessary, we use the symbol $w_\perp$ for the wall width in the state of perpendicular magnetization, to be distinguished from the wall width $w_\parallel$ that we will use later in the state of in-plane magnetization). We have some comments referring to these equations. Suppose (see Section II of SM for more details) that we fill the slab with a uniform magnetization distribution $\vec{M}=(\sin\theta,0,\cos\theta)$ (θ being the angle with respect to the z-direction). The total anisotropy energy per unit surface is given by $(-\lambda+\Omega\cdot\frac{d}{a})\cdot\cos^2\theta$. When $\lambda>\Omega\cdot\frac{d}{a}$, the state of perpendicular magnetization is the preferred one. In this state, the argument of the square roots in Eqs. 2 and 3 is positive: w and E_w have finite values. However, as $d\to d_R\doteq\frac{\lambda}{\Omega}\cdot a$, w tends to infinity and E_w to zero. Notice that spin wave excitations produce a slightly different renormalization of λ and Ω as a function of temperature and thickness [16, 17] so that d_R is itself a function of the temperature. Previous works [16, 17, 19] have established that $d_R(T)$ defines a line of phase transitions at which the perpendicular magnetization turns into the plane of the slab.

iii Absence of spontaneous magnetization and crossover length

We are now able to drive conclusions about the absence of spontaneous magnetization and crossover length. Comparing the domain wall energy cost to the magnetostatic energy gain, we recognize that the logarithmic term always favors the building of domains for sufficiently large L. Accordingly, Griffith's theorem about the absence of spontaneous magnetization in the thermodynamic limit holds true in the slab geometry with perpendicular magnetization.

One interesting outcome of our argument is the estimate of the cross-over length L_c at which a slab will transit from a monodomain state to a multidomain state, resulting from equating the magnetostatic energy gain to the wall energy:

$$L_c\approx\frac{a}{2}\sqrt{\frac{2JS^2}{\lambda-\Omega\frac{d}{a}}}\cdot\exp\left(\frac{\pi\sqrt{\left(\lambda-\Omega\frac{d}{a}\right)\cdot 2JS^2}}{\Omega\frac{d}{a}}\right). \tag{4}$$

We have some comments regarding this result. In Table 1, we observe that, sufficiently away from d_R, L_c assume values that exceed the lateral size of common laboratory samples (mm). When moving toward d_R, the exponential factor will produce L_c to decrease to few tens of micrometers (see e.g Ref. [21]). These are the lateral lengths over which exfoliated two-dimensional magnets are believed to be almost perfectly flat [6–11]. Accordingly, a sequence of exfoliated samples with suitable thickness and with increasing lateral size L should allow an insight into the yet unexplored mechanism of penetration of magnetic domains in two-dimensional ferromagnetic elements as a function of their size L. Some preliminary results in this direction were reported in Ref. [20] on epitaxially grown ultrathin films.

We point out that, closer to $d_R(T)$, the increasing width w might cause L_c to increase again. This non-monotonous behavior has no consequences regarding the no-spontaneous magnetization rule but is certainly a detail that might need further consid-

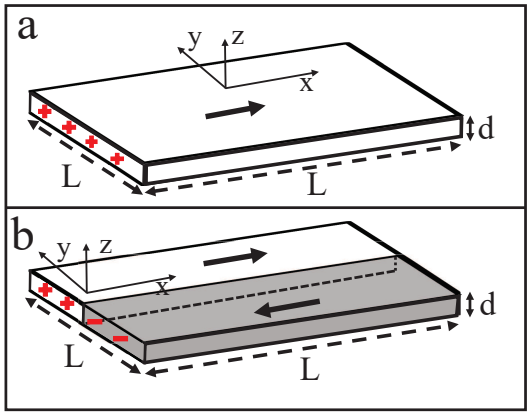

Figure 3: a: The state of uniform in-plane magnetization (represented in white) in a slab. The magnetization vector is represented by the horizontal black arrow. Effective charge densities (their sign being given in red) appear along the perimeter. b: The slab is filled by two domains with magnetization vector parallel (white domain) and antiparallel (gray domain) to the horizontal x-axis. The sign of the effective charge densities is given in red.

eration, both from the experimental and the theoretical point of view.

iv Stability against magnetic field

A final comment is dedicated to the stability against a perpendicular magnetic field of the multidomain phase that should appear at sufficiently large L. In Section IV of the SM, we analyze this problem by considering the energetics of one stripe of reversed magnetization $-M_0$, embedded into a background with magnetization $+M_0$, subject to a perpendicularly applied field with strength $+B_0$. We find that the state of uniform magnetization becomes the energetically favored one when B_0 exceeds a threshold strength $B_t \propto \mu_0 \cdot M_0 \cdot \frac{d}{L_c}$. Far away from the $d_R(T)$-transition line, the threshold field might be as small as a few nT (see Table). This means that for practical laboratory purposes, even samples with mm size appear to be single domain [21, 22]. Close to the ferromagnetic-to-paramagnetic transition line, however, the transition field is in the mT-range [21, 22].

III In-plane magnetization

We now analyze the slab geometry with in-plane magnetization. In the two configurations considered, one has uniform magnetization along, e.g., the $+x$-direction (Fig. 3a), and one has half of the slab with magnetization along the $+x$-direction and the other half with magnetization along $-x$ (Fig. 3b). In this situation, the magnetostatic energy is most appropriately computed as the Coulomb interaction between effective "charges" produced by $\vec{\nabla} \cdot \vec{M}(\vec{r})$. The charges resulting from the two spin configurations are indicated in Fig. 3 in red. The change of magnetostatic energy produced by the building of in-plane domains is negative, i.e., the magnetostatic energy favors a state of vanishing spontaneous magnetization. However, the logarithmic terms produced by the self-energies cancel out exactly when the energies of the two states are subtracted, provided the wall is parallel to the magnetization, i.e., the wall is not charged. The remaining contributions provide terms proportional to $-(\Omega \cdot d) \cdot L \cdot d$ (Section V, SM). Again, there is a wall between the two domains, in which spins rotate away from the x-direction. We assume, for simplicity, an in-plane anisotropy with the strength Λ such as the one encountered in ultrathin Fe films on W(110) [23] (see also Table 2). This anisotropy provides an energy barrier against rotations away from the x in-plane direction. Λ is not related to the breaking of translational symmetry along z and is, accordingly, much smaller than the Néel magnetic anisotropy constant forthcoming in the perpendicular magnetization configuration. Λ is rather of the same order of magnitude as the quartic in-plane magnetic anisotropy constant computed, e.g., in Ref. [14]. Given Λ, by the same arguments used in Section III of SM, the domain wall width is $w_{\parallel} \approx a \cdot \sqrt{\frac{JS^2}{\Lambda}}$ and the energy of the wall is $\approx L \cdot d \cdot 2 \cdot \sqrt{\Lambda \cdot 2 \cdot J \cdot S^2}$.

Equating the total energy change due to the formation of a domain wall to zero provides an estimate of the critical thickness d_c below which a state of spontaneous magnetization is favored:

$$d_c = \mathcal{O}\left(a \cdot \frac{\sqrt{\Lambda \cdot J \cdot S^2}}{\Omega}\right). \tag{5}$$

As L cancels out, we argue that it should be possible to find a rigorous proof of spontaneous magne-

Table 1: Summary of typical experimental and theoretical values (perpendicular magnetization). (1): Values obtained from the quoted calculations. (2): Experimental value obtained from the value for D in Ref. [18]. (3): Estimated values from the equations described in the present paper, using the values of line *1* ($d = a$). (4): fcc Fe, $a = 0.361$ nm. (5): bcc Fe on a Ag(100) surface, room temperature. (6): fcc Fe on Cu(100)($a = 0.361$ nm), at 150 K. (7): Ni on Cu(100), d between 2 to 7 nm. (8): fcc Fe on Cu(100), about 2 ML. (9): 3 ML Fe on Cu(100), room temperature (estimated from Table 1 in Ref. [30]).

Perp.	$J \cdot S^2$ [meV]	$^{\dagger}\lambda$ [meV]	$^{\ddagger}\Omega$ [meV]	$w_{\perp}$ [nm]	L_c [m]	d_R [ML]	B_t [Tesla]
(1)	$^{*}46$ [18]	0.38 [14]	0.3 [14]			1.5 [14]	
(2)	$^{*}36$ [18]						
(3)			0.28	5	$\approx 10^5$	1.26	$\approx 10^{-10}$
(4)		0.7−1.1 [16]				5-8 [16]	
(5)						6 [19]	
(6)						3 [29]	
(7)				≈ 40 [27]		10 [27]	
(8)							$\approx 10^{-3}$ [21, 22]
(9)		≈ 1 [30]					

$*$ Theoretical values for bulk bcc Fe. Realistic computations find values for the exchange interaction between atoms which are further away than nearest neighbors. The value we use here is obtained by simplifying Eq. 4.10 of Ref. [18] for the spin wave stiffness constant to $D \approx S \cdot J \cdot a^2$. An effective value for J is then obtained using the values of Table 1 in Ref. [18]. $S \approx 1.1$ [18]. † Per unit surface cell. ‡ Per bulk unit cell. Fe atoms occupying a bcc lattice, i.e., 2 atoms in the unit cell, each carrying a magnetic moment of $2.2\mu_B$ ($g \approx 2$ [18], $S \approx 1.1$ [18]). $\mu_0 = 4\pi \cdot 10^{-7} \cdot \frac{T \cdot m}{A}$, $\mu_B = 9.3 \cdot 10^{-24} \cdot \frac{\text{Joule}}{T}$, $a = 2.83 \cdot 10^{-10} \cdot m$, $1 \cdot \text{Joule} = 6.2 \cdot 10^{18} \cdot eV$.

tization even in the thermodynamic limit $L \to \infty$ in a truly 2D system with in-plane magnetization. As both states above and below d_c are stable for $L \to \infty$, the transition at d_c from a single-domain state with spontaneous magnetization to a multi-domain stripe state should be a genuine phase transition. Using the typical values for Λ, J, and Ω introduced in Table 2, we obtain $d_c \approx$ five lattice constants or less. This small number means that a sample must be fabricated with uniform thickness over large lateral distances in order for this transition to be observed. The new class of two-dimensional magnets [6–11] might provide this kind of precision. A final remark: provided that Ω, J, and Λ renormalize slightly differently with temperature, we might expect a $d_c(T)$ line of phase transitions which can also be crossed at a fixed thickness d by varying the temperature. This situation would represent the analogon to a similar phase transition observed in perpendicularly magnetized films [22].

IV Discussion of general aspects and summary of values for the parameters

An important question: in which ferromagnetic samples can the 2D-dipolar behavior in Eqs. [1-5] be detected? We recall that Eqs. [1-5] are obtained by assuming thin films ($d \ll L$) with a 2D spatial spin degree of freedom: the spin distribution is rigid along z and can only assume some profile along the xy-plane. The assumption of a spatial 2D spin profile restricts further d, which must fulfill the most stringent inequalities $d \ll w_{\perp}$ (perpendicular magnetization) and $d \ll w_{\parallel}$ (in-plane magnetization), respectively, so that any spin rotation along the z-axis is indeed suppressed. The question is now whether the 2D ferromagnetic dipolar behavior is observable within the limits of these inequalities. We argue that the range of film thickness, about which 2D dipolar behavior is best detectable, is defined by two characteristic vertical lengths: d_R (for perpendicular magnetization, see Eq.4) and d_c (for in-plane magnetization, see Eq.5). It is therefore

Table 2: Summary of typical experimental and theoretical values (in-plane magnetization). (1): Theoretical value, from Table 1. (2): Experimental values. (3): Estimated values from the equations described in the present paper, using the values in *1* and *2*. (4): 5.5 ML thick Co on Cu(100), experimental values. (5): Estimated values from the equations described in the present paper, using the values in *1* and *4*.

In-plane	$J \cdot S^2$ [meV]	Ω [meV]	Λ [meV per atom]	$w_{\|\|}$ [nm]	d_c [nm]
(1)	46 [18]				
(2)	36 [18]		$0.0026^{\dagger}$ [23]	21 [23]	
(3)		<u>0.28</u>		<u>26</u>	<u>≈ 1</u>
(4)			$\approx 10^{-5}$ [31]	≈ 500 [31]	
(5)				<u>478</u>	<u><1ML</u>

†: Experimental value. In Ref. [23], the anisotropy parameter is given as $4.5 \cdot 10^5 \frac{\text{erg}}{\text{cm}^3}$. To convert this energy in meV per atom we use 1 erg $= 6.242 \cdot 10^{11} eV$ and a density of 2 atoms per unit volume cell, with $a \approx 0.286$ nm.

required that $d \approx d_R \ll w_\perp$ and $d \approx d_c \ll w_\parallel$ for the observation of 2D dipolar behavior. Provided the anisotropy constants λ and Λ are not exceedingly large (precisely: $(\frac{\lambda}{\Omega})^2 \cdot (\lambda - \Omega) \ll S^2$ and $\Lambda \ll \Omega$), these inequalities are fulfilled. In practice, d_R and d_c depend on the material parameters and can be altered by, e.g., lattice distortion during growth [27], but their typical values are in the sub-nm to nm range (see Tables 1 and 2). $w_\perp$ and $w_\parallel$, instead, are in the 10-nm-to-100-nm range (Tables 1 and 2).

A further point of discussion is the relevance of thickness fluctuations. Ultrathin films of transition metals such as the reference system Fe on W(110) [24] are grown on top of non-magnetic surfaces, consisting of terraces with typically less than 10 nm lateral size, separated by monoatomic steps. During growth, the single layers are built from a set of flat patches that fill progressively the monolayer (for images of how the growth of Fe films on W(110) proceeds in the subnanometer thickness range, see e.g. [25]). In this growth mode (which is called "layer-by-layer" and is, accordingly, the most favorable for minimizing thickness fluctuations [26]), one observes that the final deposit has, typically, thickness fluctuations in the 1ML-to-2ML range [25]. The lateral length scale of these fluctuations is about the size of the underlying terraces, i.e., less that 10 nm. Recently obtained electron microscopy images of nm thick Ni thin films on Cu(100) [27]) show impressively the flake-like structure of these films. One could ask "therefore" how far our ideally continuous slabs can account for the magnetic properties of thin films of transition metals on non-magnetic metallic substrates. There is no conclusive and general answer to this question. It might be of help for the reader to learn that in-plane magnetized thin films, such as the reference system Fe on W(110), or perpendicularly magnetized film such as Fe on Cu(100) are, at appropriate temperatures, single domain over many μm up to mm lateral distances [21, 22, 24, 27]. One further key piece of information is that ultrathin Fe films on W(110), despite the thickness fluctuations arising from growth, undergo a very sharp ferromagnetic-to-paramagnetic 2D Ising phase transition [28], indicating that magnetic correlations are able to propagate through thickness fluctuations and to define one single "global" Curie temperature. The recent development of a new type of model systems, consisting of exfoliated 2D films that are perfectly flat over distances of a few hundred μm, is of crucial importance for this field of research because they provide a geometry closer to the ideal slab geometry discussed in this work.

We conclude the paper with two Tables (1 & 2) that summarize some typical values for the various parameters introduced in this paper and for the various derived quantities. The values derived from Eqs. 2, 3, 4, and 5 are underlined in the Tables.

Acknowledgements - We thank Dr. R. Allenspach for helping us with the references.

Supplemental Material: Details of the computations used to obtain Eqs. 1,2, 3, 4 and 5 are given online in the "Supplemental Material".

---

[1] R.B. Griffiths *Peierls Proof of Spontaneous Magnetization in a Two-Dimensional Ising Ferromagnet*, Phys. Rev., **136**, A437-A439, (1964).

[2] J. Fröhlich, B. Simon, *Infrared Bounds, Phase Transitions and Continuous Symmetry Breaking*, Commun. Math. Phys., **50**, 79-85, (1976).

[3] Jorge V. Jose, Leo P. Kadanoff, S. Kirkpatrick, David R. Nelson, *Renormalization, vortices, and symmetry-breaking perturbations in the two-dimensional planar model*, Phys. Rev. B, **16**, 1217-1241, (1977).

[4] R. B. Griffiths, *Free Energy of interacting magnetic dipoles*, Phys. Rev., **176**, 655-659, (1968).

[5] N. D. Mermin, H. Wagner, *Absence of Ferromagnetism or Antiferromagnetism in One- or Two-Dimensional Isotropic Heisenberg Models*, Phys. Rev. Lett., **17**, 1133-1136, (1966).

[6] C. Gong et al., *Discovery of intrinsic ferromagnetism in two-dimensional van der Waals crystals*, Nature, **546**, 265-269, (2017).

[7] B. Huang et al., *Layer-dependent ferromagnetism in a van der Waals crystal down to the monolayer limit*, Nature, **546**, 270-273, (2017).

[8] K. S. Burch, D. Mandrus, Je-Geun Park, *Magnetism in two-dimensional van der Waals materials*, Nature, **563**, 47-52, (2018).

[9] Yang Li, Baishun Yang, Shengnan Xu, Bing Huang, Wenhui Duan, *Emergent Phenomena in Magnetic Two-Dimensional Materials and van der Waals Heterostructures*, ACS Appl. Electron. Mater., **4**, 3278-3302, (2022).

[10] M. Gibertini, M. Koperski, A. F. Morpurgo, K. S. Novoselov, *Magnetic 2D materials and heterostructures*, Nature Nanotechnology, **408**, 408-419, (2019).

[11] Chuying Dai et al., *Research progress of two-dimensional magnetic materials*, China Mater., **66**, 859-876, (2023).

[12] Yecun Wu et al., *Interlayer engineering of Fe3GeTe2: From 3D superlattice to 2D monolayer*, Proc. Nat. Ac. Sci., **121**, (4) e2314454121 (2024).

[13] M. L. Néel, *Anisotropie magnetique superficielle et surstructures d'orientation*, J. Phys. Radium, **15**, 225-239, (1954).

[14] J. G. Gay, Roy Richter, *Spin Anisotropy of Ferromagnetic Films*, Phys. Rev. Lett., **56**, 2728-2731, (1986).

[15] J. G. Gay, Roy Richter, *Spin anisotropy of ferromagnetic slabs and overlayers*, J. Appl. Phys., **61**, 3362-3365, (1987).

[16] Long-Pei Shi, *Perpendicular magnetic anisotropy in ultrathin fcc iron films and surfaces at finite temperature*, Physics Letters A, **189**, 409-414, (1994).

[17] P. Politi, A. Rettori, M. G. Pini, D. Pescia, *Magnetic Phase Diagram of a Thin Film with a Reorientation Transition*, Europhysics Letters, **28**, 71, (1994).

[18] L. M. Small, V. Heine, *A couple method for calculating interatomic interactions in itinerant electron magnetic systems*, J. Phys. F: Met. Phys., **14**, 3041-3052, (1984).

[19] Z. Q. Qiu, J. Pearson, S. D. Bader, *Asymmetry of the Spin Reorientation Transition in Ultrathin Fe Films and Wedges Grown on Ag(100)*, Phys. Rev. Lett., **70**, 1006-1009, (1993).

[20] O. Portmann et al., *Micromagnetism in the ultrathin limit*, Thin Solid Films, **505**, 2-9, (2006).

[21] N. Saratz et al., *Critical exponents and scaling invariance in the absence of a critical point*, Nat. Commun., **7**, 13611, (2016).

[22] N. Saratz et al., *Irreversibility, reversibility, and thermal equilibrium in domain patterns of Fe films with perpendicular magnetization*, Phys. Rev. B, **82**, 184416, (2010).

[23] U. Gradmann, J. Korecki, G. Waller, *In-Plane Magnetic Surface Anisotropies in Fe(110)*, Appl. Phys. A, **39**, 101-108, (1986).

[24] S. Miesch, A. Fognini, Y. Acremann, A. Vaterlaus, T. U. Michlmayr, *Fe on W(110), a stable magnetic reference system*, J. Appl. Phys., **109**, 013905, (2011).

[25] A.-K. Thamm et al., *Hallmark of quantum skipping in energy filtered lensless scanning electron microscopy*, Appl. Phys. Lett., **120**, 052403, (2022).

[26] H. Brune, *Epitaxial Growth of Thin Films*, in "Surface and Interface Science", Editor: K. Wandelt,p.421-492, (2014), Wiley-VCH Verlag.

[27] R. Allenspach et al., *Dzyaloshinskii-Moriya interaction in Ni/Cu(001)*, Phys. Rev. B, **110**, 014402, (2024).

[28] C. Back, Ch. Würsch, A. Vaterlaus, U. Ramsperger, U. Maier, D. Pescia, *Experimental confirmation of universality for a phase transition in two dimensions*, Nature, **378**, 597-600, (1995).

[29] D. P. Pappas, K.-P. Kämper, H. Hopster, *Reversible Transition between Perpendicular and In-Plane Magnetization in Ultrathin Films*, Phys. Rev. Lett., **64**, 3179-3182, (1990).

[30] J. F. Cochran et al., *Magnetic anisotropies in ultrathin fcc Fe(001) films grown on Cu(001) substrates*, Phys. Rev. B, **45**, 4676-4685, (1992).

[31] A. Berger, H. P. Oepen, *Magnetic domain walls in ultrathin fcc cobalt films*, Phys. Rev. B, **45**, 12596-12599, (1992).